Mercury stocks in discontinuous permafrost and their mobilization by river migration in the Yukon River Basin

Smith, M. Isabel; Ke, Yutian; Geyman, Emily C.; Reahl, Jocelyn N.; Douglas, Madison M.; Seelen, Emily A.; Magyar, John S.; Dunne, Kieran B.J.; Mutter, Edda A.; More Authors

DOI
10.1088/1748-9326/ad536e

Publication date
2024

Document Version
Final published version

Published in
Environmental Research Letters

Citation (APA)
Smith, M. I., Ke, Y., Geyman, E. C., Reahl, J. N., Douglas, M. M., Seelen, E. A., Magyar, J. S., Dunne, K. B. J., Mutter, E. A., & More Authors (2024). Mercury stocks in discontinuous permafrost and their mobilization by river migration in the Yukon River Basin. *Environmental Research Letters*, *19*(8), Article 084041. https://doi.org/10.1088/1748-9326/ad536e

ENVIRONMENTAL RESEARCH
LETTERS

LETTER

Mercury stocks in discontinuous permafrost and their mobilization by river migration in the Yukon River Basin

M Isabel Smith[1,*], Yutian Ke[2], Emily C Geyman[2], Jocelyn N Reahl[2], Madison M Douglas[2,4], Emily A Seelen[1], John S Magyar[2], Kieran B J Dunne[2,5], Edda A Mutter[3], Woodward W Fischer[2], Michael P Lamb[2] and A Joshua West[1]

[1] Department of Earth Sciences, University of Southern California, Los Angeles, CA 90089, United States of America
[2] Division of Geological and Planetary Sciences, California Institute of Technology, Pasadena, CA 91125, United States of America
[3] Yukon River Inter-Tribal Watershed Council, Anchorage, AK 99501, United States of America
[4] Department of Earth, Atmospheric and Planetary Sciences, Massachusetts Institute of Technology, Cambridge, MA 02139, United States of America
[5] Delft University of Technology, 2628 CD, Delft, The Netherlands
* Author to whom any correspondence should be addressed.

E-mail: smithmi@usc.edu

Keywords: Mercury, Arctic, permafrost, erosion, Rivers

Supplementary material for this article is available online

OPEN ACCESS

RECEIVED
31 August 2023

REVISED
9 April 2024

ACCEPTED FOR PUBLICATION
3 June 2024

PUBLISHED
15 August 2024

Abstract

Rapid warming in the Arctic threatens to destabilize mercury (Hg) deposits contained within soils in permafrost regions. Yet current estimates of the amount of Hg in permafrost vary by ∼4 times. Moreover, how Hg will be released to the environment as permafrost thaws remains poorly known, despite threats to water quality, human health, and the environment. Here we present new measurements of total mercury (THg) contents in discontinuous permafrost in the Yukon River Basin in Alaska. We collected riverbank and floodplain sediments from exposed banks and bars near the villages of Huslia and Beaver. Median THg contents were $49^{+13}/_{-21}$ ng THg g sediment^{-1} and $39^{+16}/_{-18}$ ng THg g sediment^{-1} for Huslia and Beaver, respectively (uncertainties as 15th and 85th percentiles). Corresponding THg:organic carbon ratios were $5.4^{+2.0}/_{-2.4}$ Gg THg Pg C^{-1} and 4.2 $^{+2.4}/_{-2.9}$ Gg THg Pg C^{-1}. To constrain floodplain THg stocks, we combined measured THg contents with floodplain stratigraphy. Trends of THg increasing with smaller sediment size and calculated stocks in the upper 1 m and 3 m are similar to those suggested for this region by prior pan-Arctic studies. We combined THg stocks and river migration rates derived from remote sensing to estimate particulate THg erosional and depositional fluxes as river channels migrate across the floodplain. Results show similar fluxes within uncertainty into the river from erosion at both sites ($95^{+12}/_{-47}$ kg THg yr^{-1} and $26^{+154}/_{-13}$ kg THg yr^{-1} at Huslia and Beaver, respectively), but different fluxes out of the river via deposition in aggrading bars ($60^{+40}/_{-29}$ kg THg yr^{-1} and $10^{+5.3}/_{-1.7}$ kg THg yr^{-1}). Thus, a significant amount of THg is liberated from permafrost during bank erosion, while a variable but generally lesser portion is subsequently redeposited by migrating rivers.

1. Introduction

The Arctic is warming four times [1] faster than the global average, destabilizing permafrost soils that have remained frozen for two or more years and that underlie much of the Arctic [2, 3]. While moderate climate scenarios project 15%–87% permafrost loss by 2100, extreme scenarios estimate up to 99% loss [4–6]. Permafrost loss poses multiple threats to the estimated 5 million people who live in the Arctic, with 3.3 million people living in areas where permafrost is predicted to degrade and disappear by 2050 [7]. Thawing permafrost can damage critical infrastructure [8, 9], impact navigable routes [10], and decrease food security, particularly for communities with subsistence practices [10, 11].

Additionally, permafrost thaw may release contaminants that have been locked away in frozen soils for millennia [12]. The potential release of large amounts of mercury (Hg) from permafrost has received particular attention due to its threat to human health [12, 13].

Due to atmospheric circulation [14] and preservation of organics in frozen soils [9, 10], permafrost Hg has accumulated over thousands of years, and Hg in the top meter of Arctic soils potentially exceeds the total amount stored in the atmosphere, ocean, and all other soils [15–17]. However, estimates of the amount of total mercury (THg) stored in permafrost soils are poorly constrained, ranging from 184 to 755 Gg THg [15–17]. Varying estimates stem from under-sampling of Arctic soils, forcing studies to rely on sparse field data and models to determine THg stocks. Mercury to organic carbon ratios (RHgC) are often used for extrapolation due to relatively more abundant carbon data availability and first-order correlation between Hg and carbon in many settings. However, RHgC are in fact highly variable ($\tilde{x} = 2.0 \pm 1.9$ [15],) and need to be better constrained for their use as a Hg proxy across Arctic soil types. Additionally, existing THg stock measurements are limited to the top 3 m, primarily due to practical limitations of soil coring, even though deeper sediments may be important stores of Hg and other constituents [18].

Quantifying Hg stocks and understanding their remobilization to biologically active zones is important as liberation of this Hg during permafrost thaw could be detrimental to Arctic communities. A proportion of mobilized inorganic Hg (∼1% in the Yukon River Basin (YRB)) is bacterially transformed into methylmercury [19], a neurotoxin that bioaccumulates in organisms, affecting animal and human health when consumed [20–24]. Many Indigenous communities, including Alaska Native communities, rely on subsistence fishing and have disproportionately elevated blood Hg levels linked to dietary exposure [25, 26]. Altering Hg inputs to Arctic waterways has an immediate and direct impact on Hg exposure in these communities, as well as affecting the Hg delivered to ecosystems and the Arctic Ocean.

Despite its potentially deleterious effects, the mobility of Hg during thaw are not well understood. A range of processes can release Hg from permafrost, including gaseous evasion [27], aqueous leaching [13, 19], and river erosion which can quickly mobilize large amounts of sediment [17, 28, 29]. To better constrain floodplain THg stocks and quantify release from erosion of permafrost deposits, we present a new dataset of THg measurements in riverbank and floodplain sediments. We also employ a mass balance approach to evaluate the role of net river migration on erosional and depositional THg sediment fluxes in the YRB of Alaska.

2. Methods

2.1. Sampling sites

The YRB spans more than 330 000 km^2 in regions of northwestern Canada and central Alaska and is underlain by areas of continuous and discontinuous permafrost [30]. The Yukon River has the highest flow-weighted annual THg concentration out of the six major Arctic rivers [29], and the YRB is one of the six major freshwater contributors to the Arctic Ocean, supplying 3–32 times more THg to the oceans than the 8 other major northern hemisphere river basins [19]. This makes the YRB an important focus of study in the context of riverine THg inputs in a changing Arctic.

Yukon river waters contain a range of sediment sizes, which are expected to influence organic carbon (OC) and Hg contents. To capture some of this variability, we focused on two regions in the YRB underlain by discontinuous permafrost with distinct riverbed sediment characteristics (figure 1). Our sites were chosen near Alaska Native communities that are at different risk levels for erosion, flooding, and permafrost thaw [31, 32] to coincide with overarching collaborative efforts to understand the effects of erosion in the YRB. At both sites, the river channel migrates laterally through cutbank erosion and point bar deposition at rates of meters per year [33].

2.2.1. Field sampling procedures

Sediment samples were collected from exposed riverbanks and pits dug (∼0.5–1 m deep) into point bar deposits (figures 1(B), (C) and supplementary, text S1). Stratigraphic columns were measured from the top of the bank to the waterline or from the top of the pit to the bottom of the pit, which was usually frozen ground. Descriptions of stratigraphic columns, distinct bed thickness, sample depth, and substrate class (gravel, sand, peat, mud) were recorded. The surficial 5–10 cm of exposed sediments were removed before sample collection. Paired samples were collected for analysis of geochemistry and bulk density (details in supplement, text S1). At selected permafrost cutbanks, we sampled both thawed material on the surface (effectively the 'active layer' of material exposed on the vertical bank) and frozen material recovered by drilling into the bank with a hole saw.

2.2.2. Lab analysis

Sediment samples for geochemical analysis were freeze dried and split. Geochemical subsamples were ground into a homogeneous fine powder in an agate

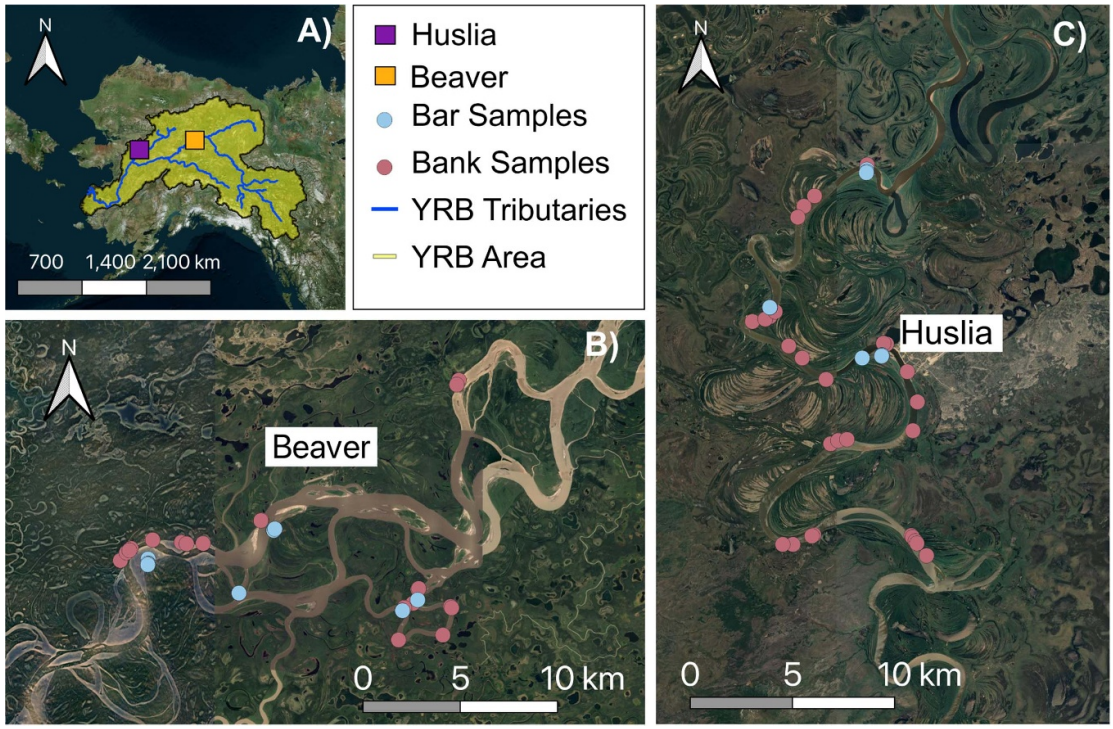

Figure 1. Study sites located in interior Alaska in the YRB (watershed boundary-yellow shaded region [34], tributaries-blue line) (A). Samples were collected along an anastomosing, gravel-bedded reach of Yukon River (B) and a sand-bedded reach of the Koyukuk River (C), a single-threaded meandering river that is a major tributary of the Yukon River. Sampling locations were located near the villages of Huslia (purple square in A) and Beaver (orange square in A). Dots represent cutbanks (red; $n = 56$) and point bars (blue; $n = 29$) that have been characterized. Samples were collected in June 2022 (Huslia: 18 cutbanks, 6 point bars; Beaver: 13 cutbanks, 6 point bars) and September 2022 (Huslia: 15 cutbanks, 8 point bars; Beaver: 10 cutbanks, 6 point bars) (supplementary, dataset S1). To capture a holistic view of the floodplain, sites were selected to span a range in ages, terrain type, and permafrost presence determined from geomorphic maps [33, 35, 36]. Seasonal variation in water level affected sampling site accessibility, so sites from June and September are complimentary, but not identical.] (A) Microsoft® Bing™ Maps Platform screen shot(s) reprinted with permission from Microsoft Corporation [37]. Yukon River Watershed Boundary shapefile reproduced [34] with permission from Yukon River Inter-Tribal Watershed Council. (B) and (C) Map data: Google, Maxar Technologies, CNES/Airbus, Landsat/Copernicus [38].

mortar and pestle (supplementary, text S2). THg contents were determined using a NIC direct mercury analyzer (MA-3000) at the University of Southern California using the United States Geological Survey Mercury Research Laboratory protocol [39, 40]. Analysis of reference material MESS-4 (90 ± 40 ng g^{-1}, National Research Council Canada) showed a median value of 64.9 ± 2.6 ng Hg g^{-1} (supplementary, figure S1, with uncertainty reported as relative standard deviation, or RSD) and blanks were below detection. All sediment samples were run in multiples (100% duplicate, 18% triplicate; median RSD of 2.03%) (supplementary, figures S1 and S2).

Total organic carbon (TOC) content was analyzed using an Elementar elemental analyzer at Woods Hole Oceanographic Institute's National Ocean Sciences Accelerator Mass Spectrometry Facility (NOSAMS, [41]). 38% of samples were analyzed in duplicate, yielding a median RSD of 5%. The analytical precision was assumed to be less than 1%. TOC (wt%) and THg content were used to calculate RHgC, reported as μg Hg g C^{-1} [40, 41]. Bulk density samples were weighed pre- and post-oven drying (80 °C) to determine water mass fraction and dry density. Samples were categorized visually using a grain-size card into substrate classes of sand, mud, peat, and gravel. For each field site, THg content and RHgC values were sorted by substrate composition and a one-way ANOVA test ($a < 0.05$) was conducted to determine if substrate compositions were statistically different from each other.

2.2.3. Stock calculations

We calculated THg stocks for the most complete stratigraphic sections sampled (Huslia: 15 cutbanks and 11 bars; Beaver: 13 cutbanks and 16 bars, supplementary, table S1). Near-surface stocks were determined by integrating over 1 meter and 3 m depth to compare with previously published datasets [15–17]. Total stocks that can potentially be reworked by river lateral migration were determined for the full column depth (~10–15 m), defined as the distance from the top of the cutbank (CB) or point bar (PB) to the bottom of the thalweg (the deepest part of the river). However, incomplete bank exposure and inability to dig below the thawed active layer meant we could not

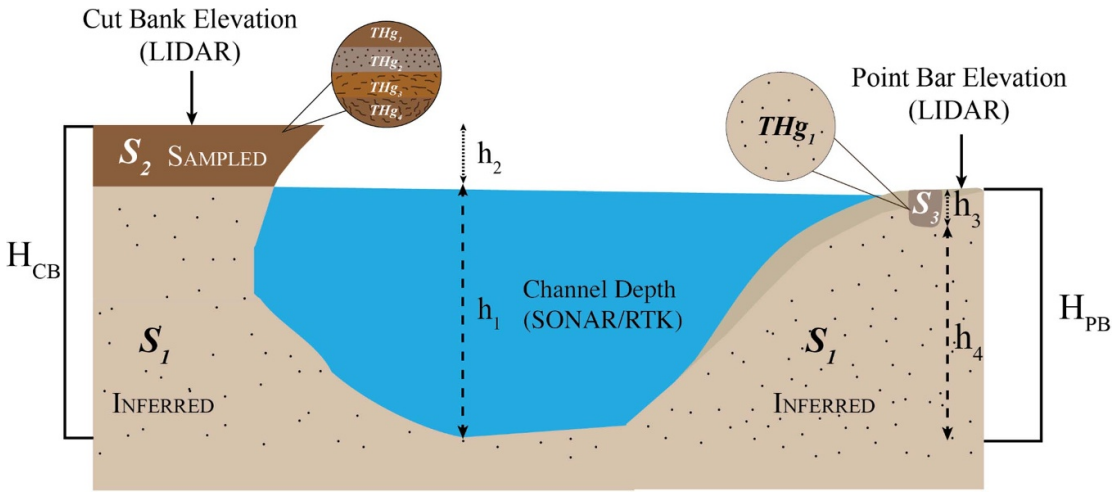

Figure 2. Schematic showing different components of the THg stock (S) calculation and where the data for each variable was obtained. Sampled sections were directly measured in the field, while inferred sections were determined using average values based on substrate composition (supplementary, tables S1 and S4). S_2 represents the sampled cutbank stock, with h_2 the corresponding exposed height. S_3 represents the sampled point bar stock, accessed by digging a pit, with h_3 representing associated depth.

sample below the top ∼20%–50% of this sedimentary column. Thus, we estimated full column stocks for PB and CB by the sum of the sampled and inferred stocks for each stratigraphic layer in the column (i) (equation (1), supplementary, table S1)

$$S_{\text{PB or CB}} = \sum_{i=1}^{n} \rho_{\text{dry},i} * h_i * \text{THg}_i. \quad (1)$$

For exposed sections of bank and bars, sampled stocks were directly calculated using measured layer thicknesses (h_i, km) from each identifiably stratigraphic layer, dry density of bank material (ρ_{dry}, kg dry sediment km^{-3}) and THg mass fraction (THg$_i$, kg Hg kg dry sediment^{-1}) from collected paired samples. Any missing stratigraphic information was supplemented with an average value from sediments of similar substrate composition from the same field location (supplementary, tables S2 and S3).

To calculate THg stocks for the unsampled sections (the 'inferred' portion in figure 2), we determined unsampled column heights and inferred associated sediment properties. Total column heights, independent of river stage height, were determined based on bathymetric and elevation data (supplementary, table S1). Bathymetry was mapped via SONAR surveys at the time of sample collection, referenced by RTK-GPS (real-time kinematic geographic positioning system). Topography data were from National Center for Airborne Laser Mapping Light Detection and Ranging datasets from flights over Huslia on 21–23 August 2022, and over Beaver on 2–5 August 2021 (figure 2). The sampled sections (h_2, h_3) were subtracted from total column height (H$_{\text{CB}}$, H$_{\text{PB}}$) to determine the unmeasured section (h_1, h_4) heights.

To infer sediment properties, we used our most complete stratigraphic sections (∼5–10 m thick), measured in late fall when the Koyukuk (Huslia) and Yukon (Beaver) Rivers were at low stage. We determined that 3 m was a characteristic maximum thickness for fine-grained overbank sediments at both sites (supplementary, figure S3). We then bootstrap resampled all measured beds below 3 m depth from the modern floodplain surface to estimate sediment properties of all unmeasured beds. We found that lower beds (>3 m) were predominantly sand in Huslia and a mixture of gravel and sand in Beaver (supplementary, figure S4). Our findings of grain size fining upward is typical of river lateral accretion deposits [42]. We calculated inferred section stocks using an average dry density and THg content (supplementary, table S4) based on substrate composition for each location.

2.2.4. Flux calculations

To calculate the flux of sediment-bound THg going into and out of the river, we created a one-dimensional mass balance box model (supplementary, figure S5) representative of erosion and deposition along our study reaches within the Koyukuk and Yukon Rivers following prior work on OC [43] in the same region. For our most complete stratigraphic sections, we calculated THg fluxes for individual banks and bars (supplementary, table S5) following:

$$F = L * k * S_x \text{ where } x = \text{CB, PB}. \quad (2)$$

Cutbank erosion and point bar deposition flux (F, kg Hg y^{-1}) for Huslia and Beaver were calculated using site-specific river migration rates (k, km y^{-1})

calculated from 10 m resolution Sentinel-2 satellite imagery over the period 2016–2022 [44], THg stocks (S_x, kg Hg km^{-2}), and river reach lengths (L, km) of the entire study areas. Huslia had river reach length of 58 km with migration rates ranging from 0.63–7.6 m y^{-1}, while Beaver had migration rates of 0.10–12 m y^{-1} along the 55 km river reach (supplementary, figure S6, tables S4 and S5, [44]). Uncertainties were estimated via a bootstrapping resampling simulation ($n = 10\,000$), selecting random calculated bank and bar fluxes to calculate a median net mercury flux; uncertainties are reported as 15th and 85th percentiles of the resulting distributions. The net flux (F_{net}) from river migration was calculated based on the difference between cutbank (F_{CB}) and point bar (F_{PB}) fluxes, as:

$$F_{net} = -F_{CB} + F_{PB}. \quad (3)$$

This approach only quantifies loss or gain of Hg from a river reach due to floodplain erosion and deposition; it does not consider sediment imported from upstream and exported downstream, and as such does not capture all processes mobilizing Hg across the watershed.

3. Results

3.1. Sediment THg content and RHgC

The median THg content was $49^{+13}/_{-21}$ ng Hg g sediment^{-1} and $39^{+16}/_{-18}$ ng Hg g sediment^{-1} (figure 3, uncertainties reported as 15th and 85th percentiles) for Huslia and Beaver, respectively. The median RHgC for Huslia was $5.4^{+2.0}/_{-2.4}$ μg Hg g^{-1} C and $4.2^{+2.4}/_{-2.9}$ μg Hg g C^{-1} for Beaver (figure 3). Where we collected paired samples of thawed and frozen material from cutbanks, THg contents were generally lower in the frozen material in Huslia and Beaver had no apparent trends (supplementary **table S6**). We cannot rule out contamination from the hole saw used to sample frozen material as contributing to the differences in Huslia, but effort was made to remove material that had come into contact with metal during sample collection.

Across all of the samples analyzed, THg content showed no apparent trends with depth (figure S7) and a positive relationship to TOC (figures 4(A) and (D)) and substrate class (p-values < 0.0001, figures 4(B) and (E)). RHgC showed a negative relation to TOC (figures S8(C) and (F)) and substrate class (p-values < 0.0001, figures 4(C) and (F)). These results suggest that THg contents in these systems are strongly correlated to substrate class and OC content.

3.2. Hg stocks and fluxes

The median heights of the complete stratigraphy from banktop to the channel thalweg at Huslia were 11 m for cutbanks and 10 m for point bars; depths at Beaver were 12 and 11 m, respectively. Median cutbank stocks at Huslia were 41 $^{+6}/_{-20}$, $125^{+44}/_{-62}$, and $327^{+123}/_{-39}$ kg Hg km^{-2}, over 1 m, 3 m, and total depths, respectively (figure 5). Equivalent point bar THg stocks at Huslia were $33^{+4}/_{-11}$, $90^{+4}/_{-11}$, and $250^{+7}/_{-63}$ kg Hg km^{-2}. At Beaver, cutbank stocks were $36^{+13}/_{-8}$, $103^{+28}/_{-18}$, and $337^{+44}/_{-76}$ kg Hg km^{-2}, while point bar stocks were $29^{+6}/_{-4}$, $92^{+4}/_{-6}$, and $274^{+37}/_{-85}$ kg Hg km^{-2}. Point bar and cutbank stocks at both Huslia and Beaver overlapped within uncertainty for most depth intervals (figure 5). The bimodal distributions of THg stocks observed in figures 6(C)–(E) are due to the point bar elevation differences between sites.

The median fluxes at Huslia were 95 $^{+12}/_{-47}$ and 60 $^{+40}/_{-29}$ kg Hg yr^{-1} for cutbank erosion and point bar deposition, respectively. Beaver had corresponding median fluxes of 26 $^{+154}/_{-13}$ and $10^{+5.3}/_{-1.7}$ kg Hg yr^{-1}. The net THg budget associated with river migration for Huslia ($+32^{+28}/_{-29}$ kg Hg yr^{-1}, reflecting net deposition of THg in point bars) and Beaver ($-17^{+9}/_{-7}$, reflecting net erosion of THg into the river) were calculated as the difference between the median erosion and deposition fluxes, with uncertainties estimated by bootstrap resampling with replacement. Overall, both sites showed similar fluxes of THg release by cutbank erosion, overlapping within uncertainty. However, the THg flux from point bar deposition is significantly higher at Huslia than at Beaver, leading to different estimates of the net budgets.

4. Discussion

4.1. Stocks

This study presents new THg and RHgC measurements (supplemental dataset 1) from the YRB using a spatially dense sampling approach that allows us to determine regional THg stocks with accuracy not possible with prior, more generalized approaches. Median THg values for Huslia and Beaver are similar to those reported in prior studies from Alaska as well as other settings in the Arctic ([15–17]; figure 3).

THg stocks for the upper 3 m are similar to those predicted for our study region in the map produced by Schuster *et al*, who used OC datasets and the RHgC to determine Pan-Arctic THg stocks ([15], figure 5). The consistency of our stock calculations with their predictions may be unsurprising since their model was based on samples collected from interior Alaska. However, our RHgC values were higher than reported in their study and other Arctic studies (figure 3, [15–17]), primarily because of lower OC at our sites. Interestingly, lower carbon content is not reflected in lower THg content in these sediments despite the

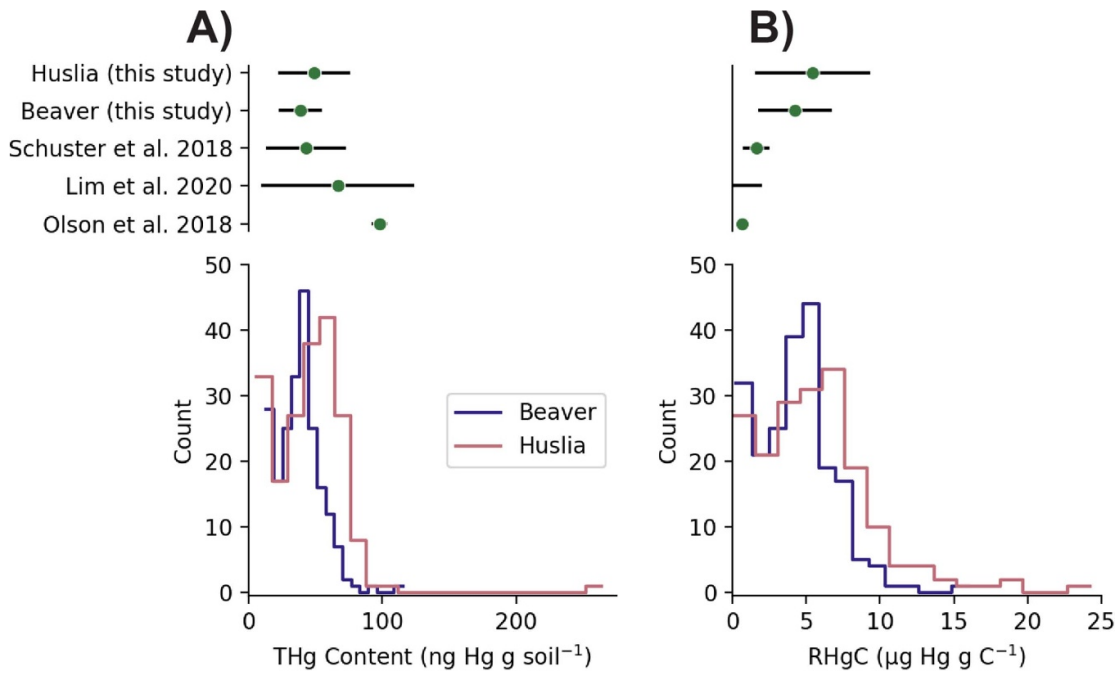

Figure 3. Median (A) THg and (B) RHgC values from this study and similar pan-Arctic studies (Alaska: Schuster and Olson; Siberia: Lim), with histograms from this study for comparison. Green dots represent the median value and black error bars show the uncertainty in the median from each study. Sample range in RHgC is given for Lim et al. 2020, as no median was reported.

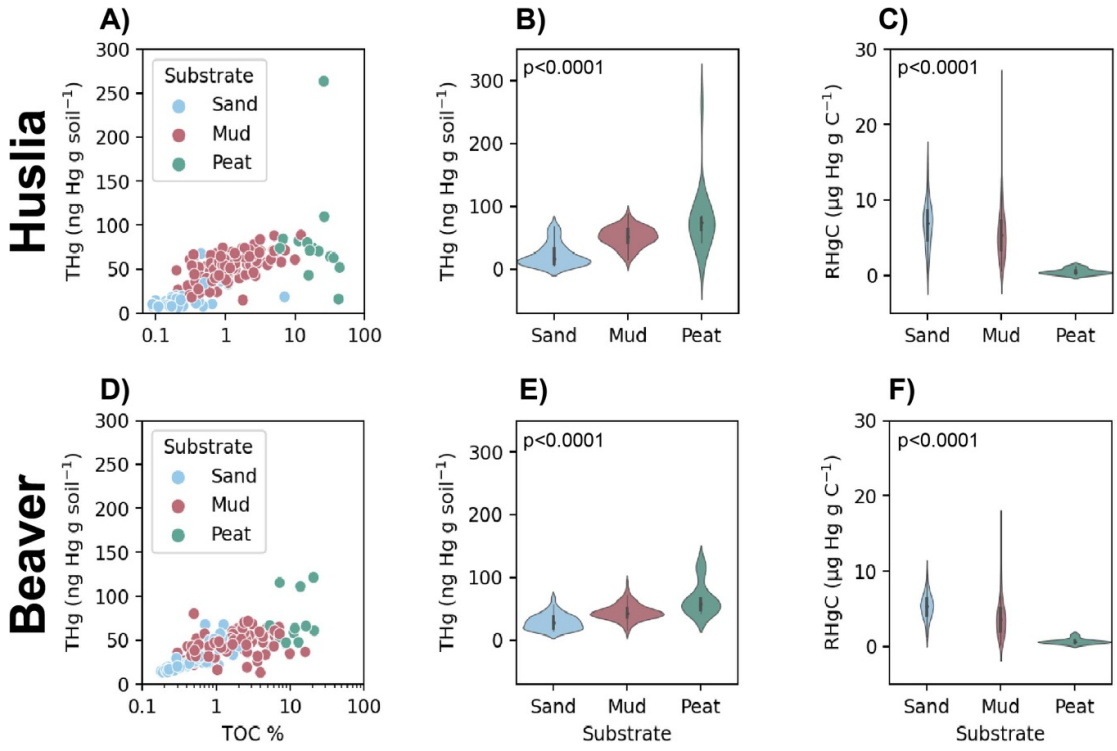

Figure 4. Comparison of THg to TOC% (A), (D) and substrate composition to THg contents (B), (E) and RHgC (C), (F) for Huslia and Beaver. Plots show all 413 samples collected in June and September 2022. THg and RHgC in relation to substrate classes all had $p < 0.0001$.

expected association of Hg and OC. The end result of similar stock values emerges by the coincidence of higher RHgC values and lower OC content in our samples, so even though the studies converge on similar final numbers, we find underlying sediment chemistry that is notably different than predicted.

We find variable RHgC both across sites and with depth (supplementary figure S8). Similar to another

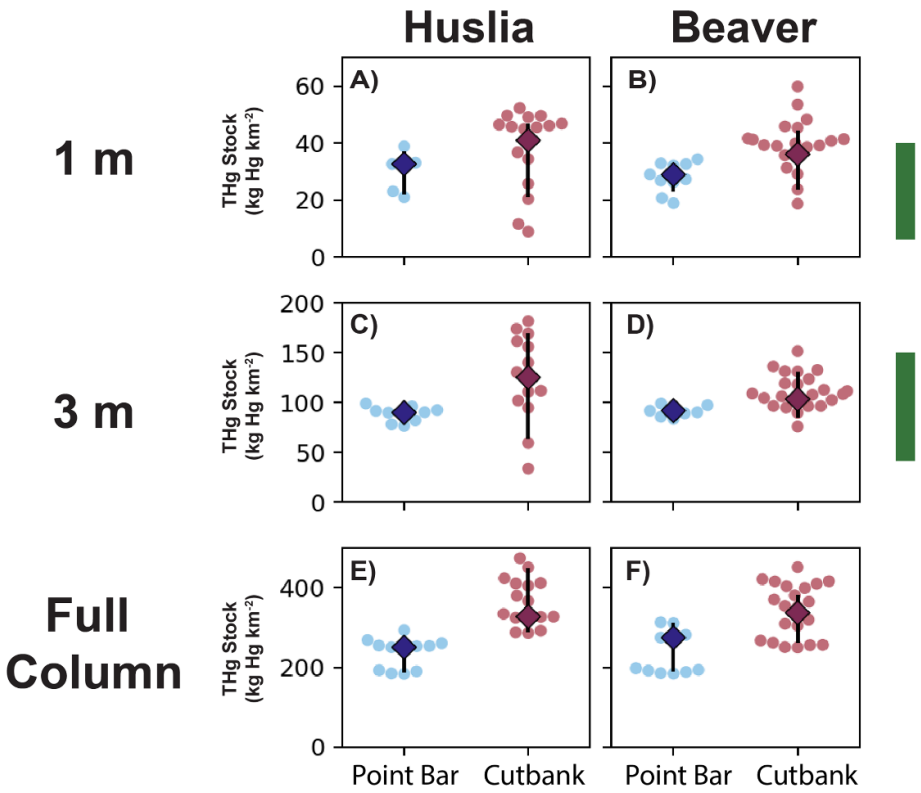

Figure 5. Estimates of THg stocks at depth intervals of 1 m (A), (B), 3 m (C), (D), and bank full depth (E), (F) for Huslia and Beaver. Dots represent individual banks (Beaver: $n = 13$, Huslia: $n = 15$) or point bars (Beaver: $n = 16$, Huslia: $n = 11$), while diamonds represent the median of all banks or bars. Error bars represent the 15th and 85th percentiles. Stocks from columns with >30% unmeasured layers were excluded from figure (supplementary table S1, figure S9). Green bars represent the THg stock (top 1 m: 6–40 kg Hg km^{-2}, top 3 m: 41–150 kg Hg km^{-2}) inferred for the study region from global maps of permafrost THg [15].

Arctic study [18], substrate composition plays an important role in soil THg content (figures 4(B) and (E)) and has an even stronger influence on RHgC values (figures 4(C) and 5(F)). We find few samples with very high OC, and variable soil composition could be a simple explanation for the variable RHgC values—particularly in the case of our peat samples. Our sites were dominated by low OC mineral soils and many of the peat samples were found as laminae in silty layers. It is possible that during formation, periodic river floods allowed water to deposit fine mineral sediment into the peat pore spaces. Thus, samples that appear to be peat may have high mineral soil composition, diluting the percentage of OC. Understanding the causes of varying RHgC in Arctic soils, e.g. via micro-analysis to look at mineral and OC-phase associations of Hg, could be a valuable target for future work. In any case, our results highlight that incorporating sedimentological controls on THg contents and RHgC ratios, and their spatial variability, in models will likely improve estimates of THg stored in permafrost.

Point bar and cutbank stocks in both Huslia and Beaver overlap within uncertainty for most depth intervals (figure 5), although in all cases the median values for cutbanks are higher than for point bars and in some cases the difference is statistically significant. For the full sediment column depth, the cutbank and point bar THg stocks are significantly different at both sites (Beaver $p < 0.001$, Huslia $p < 0.001$). These differences could be explained by the difference in elevation and age of the features: cutbanks have had more time to develop topsoil and accumulate peat in addition to fine grained sediments from overbank deposition, while point bars are lower in elevation and consist of coarser sediment in the top few meters.

4.2. Migration and mobility

Abrupt thaw events can rapidly mobilize meters-thick deposits of sediment, potentially releasing the large Hg stores in permafrost. For example, thaw slumps adjacent to a tributary of the Mackenzie River in Canada were shown to elevate suspended particulate Hg contents downstream, but river Hg loads decreased once the particles settled out of the water column [28]. Our results, based on riverbank stocks, reveal the integrated effects of erosion and sedimentation along multiple eroding bends of the Yukon and Koyukuk Rivers. The nearly balanced THg stocks between cutbanks and point bars in our study suggest that most THg eroded from the banks during river migration is redeposited with sediments in aggrading

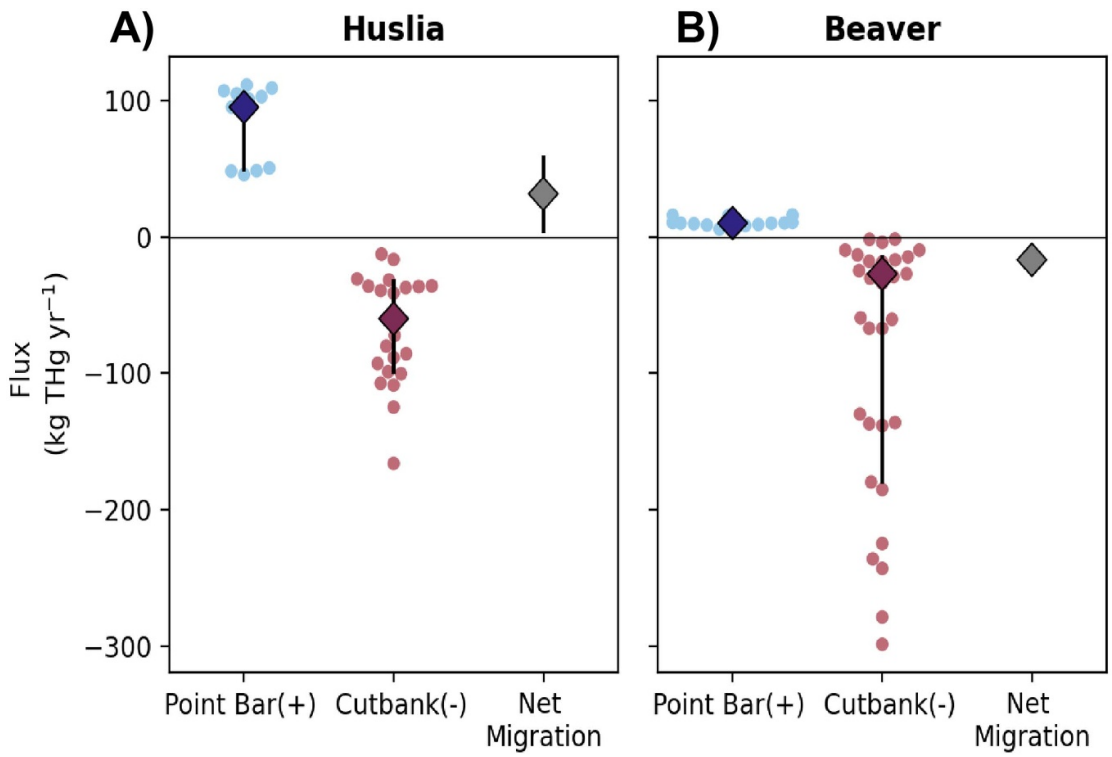

Figure 6. Mercury fluxes from the river to the floodplain (positive direction) due to point bar deposition and cutbank erosion, and the net effect of river migration, for Huslia (A) and Beaver (B). Dots represent individual calculated bank and bar fluxes while diamonds represent median fluxes. Error bars for point bars and cutbanks are the 15th and 85th percentiles. Error bars for net migration were calculated using a bootstrap resampling method ($n = 10\,000$).

bars (figure 6), similar to the Mackenzie River slump study [28].

In principle, the sediment budget of cutbank erosion and point bar deposition should be balanced along the river if the river channel is maintaining a constant width over time [45]. Any imbalance would lead to widening (if erosion outpaces deposition) or narrowing over time (if deposition exceeds erosion). If we assume the flux of sediment into the river from erosion is balanced by the flux out of the river via deposition, then comparing the THg in sediment on eroding banks and depositing point bars reveals the net THg flux associated with riverbank erosion. This framework has been applied to OC fluxes along the Koyukuk River near Huslia [43]. With this approach, we find a net release of Hg from the floodplains to the rivers, because the full column stocks on eroding cutbanks have higher THg than aggrading point bars (figure 5).

We can also relax the assumption of equal rates of bank erosion and deposition, and instead base these fluxes on observed local migration rates from satellite imagery [44], as used to calculate the THg fluxes in figure 6. In this case, the apparently more rapid accretion of point bars at Huslia compared to eroding cutbanks leads to a calculated net deposition of THg from the river into sedimentary deposits. In contrast, high rates of cutbank erosion at Beaver (figure 6) lead to a net erosional release of THg to the river. This spatial difference—with one site exhibiting apparent net Hg erosion and the other deposition—emerges from different erosion rates, emphasizing the importance of quantifying such rates and their spatial variability for understanding biogeochemical responses in a changing Arctic. While satellite-based migration rates may capture a more accurate picture of recent changes over our study sites than assuming balanced erosion and deposition, satellite observations are inherently limited in their time and length scales [46]. Imbalances in erosion and deposition cannot be sustained indefinitely and may not hold over longer reaches of the Yukon and Koyukuk Rivers.

The fluxes per unit river length associated with bank erosion and deposition that we calculate for Huslia and Beaver are 0.6 and 0.3 kg Hg km^{-1} yr^{-1}. The Yukon River delivers 4400 kg Hg yr^{-1} to the Arctic Ocean [19], which would equate to 1.38 kg Hg km^{-1} yr^{-1} just based on the main stem length of ~3200 km. While we recognize that many tributaries contribute to the Yukon (including the Koyukuk) and there are many other sources of Hg to the river across its watershed, this simple comparison reveals that the magnitude of Hg exchange between bank and bar sediments is significant in the context of Yukon River Hg transport. If exchange fluxes in our study areas (figure 6) are representative of the river as a

whole, then our results imply that there could be complete exchange of particulate Hg between the river and floodplain over the length of the Yukon. Warming climate is expected to cause permafrost loss and change upland hydrological dynamics, which in turn may alter the pace of this exchange and potentially allow for erosion to outpace deposition. Given the magnitude of the floodplain exchange fluxes, such changes could lead to significant net Hg mobilization from floodplain deposits.

As we find that significant Hg is being eroded in some areas and deposited in others, understanding the extent of Hg mobilization to rivers and its impacts will depend on local sampling because monitoring at a small number of gauging stations may not capture evolving dynamics of Hg mobilization in a changing climate. For example, in the Rio Bermejo, a tributary of the Paraguay River in northern Argentina, water flows through the ∼1200 km channel in 14 d, while sediments take on average ∼8500 years [47]. During transport, sediments undergo ∼4.5 erosion-deposition events, each taking ∼1900 years [48]. In comparison, the Koyukuk spans ∼645 km and the Yukon ∼3200 km [30]. As both of these rivers are experiencing active erosion and deposition, it may take decades or longer for geochemical signals to make it to Pilot Station where most river chemistry observations are made on the Yukon River. Our results thus highlight the importance of accurately capturing the dynamics of erosion and deposition for understanding Hg transport in Arctic rivers and how they will evolve in a changing climate.

5. Conclusions

To ground-truth Arctic Hg stocks and evaluate the role of river erosion and deposition in determining particulate Hg fluxes, we conducted two field campaigns along the Koyukuk and Yukon Rivers near the villages of Huslia and Beaver, Alaska, in June and September 2022. We report a median THg $49^{+13}/_{-21}$ ng Hg g soil^{-1} (15th and 85th percentile) ($n = 195$) and a median RHgC of $5.4^{+2.0}/_{-2.4}$ μg Hg g C^{-1} ($n = 186$) for sediment samples collected in Huslia and a median THg of $39^{+16}/_{-18}$ ng Hg g soil^{-1} ($n = 218$) and a median RHgC of $4.2\ ^{+2.4}/_{-2.9}$ μg Hg g C^{-1} ($n = 209$) for Beaver. We find that THg content was generally higher in sediment with finer grains than coarser grains. Using collected samples and bank stratigraphy characterized in the field, we calculated Hg stocks for 28 banks and 27 bars. Median stock calculations for Huslia and Beaver were generally within the range expected for our study sites based on Pan-Arctic THg models [15].

Following the framework that the rivers are maintaining constant width, our significantly larger THg stocks on eroding cutbanks in comparison to aggrading point bars imply net release of THg via erosion at both sites. However, on shorter timescales, satellite-derived migration rates suggest that the rivers might not maintain constant channel width. We observe faster rates of deposition in Huslia, yielding net THg deposition, and faster rates of erosion in Beaver, suggesting net THg release. Since the magnitude of calculated fluxes are significant at the scale of the YRB, our findings suggest that accounting for river migration rates, at least on shorter time scales, is critical for assessing changes to Hg transport in Arctic rivers.

Data availability statement

The data that support the findings of this study are openly available at the following URL/DOI: 10.18739/A2FX74076.

Acknowledgments

This work was supported by the National Science Foundation (Grant Numbers: #2127442, #2127444, and #2127445), the Geological Society of America, and the Resnick Sustainability Institute at Caltech. We thank the Beaver Village Council and the Huslia Tribal Council for their invaluable support and the opportunity to work on their lands. We also thank our boat drivers and bear guards for guiding us: Alvin Attla, Darin Dayton, Shawn Huffman, Kody Vanderpool, Richard Williams, and Clinton Wiehl. Finally, we thank Rain Blankenship for processing sediment samples and Justin Nghiem and Hannah Dion-Kirschner for assistance in the field.

ORCID iDs

M Isabel Smith https://orcid.org/0009-0002-9170-7222
Yutian Ke https://orcid.org/0000-0002-9098-9419
Emily C Geyman https://orcid.org/0000-0003-4349-9350
Jocelyn N Reahl https://orcid.org/0000-0001-5544-2138
Madison M Douglas https://orcid.org/0000-0002-0762-4719
Emily A Seelen https://orcid.org/0000-0003-3782-9341
John S Magyar https://orcid.org/0000-0002-3586-8286
Kieran B J Dunne https://orcid.org/0000-0003-0995-7629
Edda A Mutter https://orcid.org/0000-0002-1681-8080
Woodward W Fischer https://orcid.org/0000-0002-8836-3054
Michael P Lamb https://orcid.org/0000-0002-5701-0504
A Joshua West https://orcid.org/0000-0001-6909-1471

References

[1] Rantanen M, Karpechko A, Lipponen A, Nordling K, Hyvärinen O, Ruosteenoja K, Vihma T and Laaksonen A 2022 The Arctic has warmed nearly four times faster than the globe since 1979 *Commun. Earth Environ.* **3** 168

[2] van Everdingen R O 2005 Multi-Language Glossary of Permafrost and Related Ground- Ice Terms in Chinese, English, French, German, Icelandic, Italian, Norwegian, Polish, Romanian, Russian, Spanish, and Swedish (available at: https://globalcryospherewatch.org/reference/glossary_docs/Glossary_of_Permafrost_and_Ground-Ice_IPA_2005.pdf) (Accessed 1 August 2023)

[3] Osterkamp T E and Romanovsky V E 1999 Evidence for warming and thawing of discontinuous permafrost in Alaska *Permafr. Periglac.* **10** 17–37

[4] Koven C D, Riley W J and Stern A 2013 Analysis of permafrost thermal dynamics and response to climate change in the CMIP5 Earth system models *J. Clim.* **26** 1877–900

[5] McGuire A D *et al* 2018 Dependence of the evolution of carbon dynamics in the northern permafrost region on the trajectory of climate change *Proc. Natl Acad. Sci.* **115** 3882–7

[6] Chadburn S E, Burke E J, Cox P M, Friedlingstein P, Hugelius G and Westermann S 2017 An observation-based constraint on permafrost loss as a function of global warming *Nat. Clim. Change.* **7** 340–4

[7] Ramage J, Jungsberg L, Wang S, Westermann S, Lantuit H and Heleniak T 2021 Population living on permafrost in the Arctic *Popul. Environ.* **43** 22–38

[8] Arctic Monitoring and Assessment Programme 2021 Arctic climate change update 2021: key trends and impacts *Summary for Policy-Makers* (Arctic Monitoring and Assessment Programme (AMAP)) pp 1–16 (available at: https://www.amap.no/documents/download/6759/inline)

[9] Bronen R 2013 Climate-induced displacement of Alaska native communities (The Brookings Institution) p 25 (available at: https://www.brookings.edu/wp-content/uploads/2016/06/30-climate-alaska-bronen-paper.pdf)

[10] Berkes F and Jolly D 2001 Adapting to climate change: social-ecological resilience in a Canadian Western Arctic Community *Conserv. Ecol.* **5** art18

[11] Wesche S D and Chan H M 2010 Adapting to the impacts of climate change on food security among Inuit in the Western Canadian Arctic *EcoHealth* **7** 361–73

[12] Miner K R, D'Andrilli J, Mackelprang R, Edwards A, Malaska M J, Waldrop M P and Miller C E 2021 Emergent biogeochemical risks from Arctic permafrost degradation *Nat. Clim. Change.* **11** 809–19

[13] Schaefer K, Elshorbany Y, Jafarov E, Schuster P F, Striegl R G, Wickland K P and Sunderland E M 2020 Potential impacts of mercury released from thawing permafrost *Nat. Commun.* **11** 4650

[14] Durnford D, Dastoor A, Figueras-Nieto D and Ryjkov A 2010 Long range transport of mercury to the Arctic and across Canada *Atmos. Chem. Phys.* **10** 6063–86

[15] Schuster P F *et al* 2018 Permafrost stores a globally significant amount of mercury *Geophys. Res. Lett.* **45** 1463–71

[16] Olson C, Jiskra M, Biester H, Chow J and Obrist D 2018 Mercury in active-layer tundra soils of Alaska: concentrations, pools, origins, and spatial distribution *Global Biogeochem. Cycles* **32** 1058–73

[17] Lim A G, Jiskra M, Sonke J E, Loiko S V, Kosykh N and Pokrovsky O S 2020 A revised pan-Arctic permafrost soil Hg pool based on Western Siberian peat Hg and carbon observations *Biogeosciences* **17** 3083–97

[18] Rutkowski C *et al* 2021 Mercury in sediment core samples from deep Siberian ice-rich permafrost *Front. Earth Sci.* **9** 718153

[19] Schuster P F, Striegl R G, Aiken G R, Krabbenhoft D P, Dewild J F, Butler K, Kamark B and Dornblaser M 2011 Mercury export from the Yukon River Basin and potential response to a changing climate *Environ. Sci. Technol.* **45** 9262–7

[20] López-Berenguer G, Peñalver J and Martínez-López E 2020 A critical review about neurotoxic effects in marine mammals of mercury and other trace elements *Chemosphere* **246** 125688

[21] Chang L W 1977 Neurotoxic effects of mercury—a review *Environ. Restor.* **14** 329–73

[22] Campbell L M, Norstrom R J, Hobson K A, Muir D C G, Backus S and Fisk A T 2005 Mercury and other trace elements in a pelagic Arctic marine food web (Northwater Polynya, Baffin Bay) *Sci. Total Environ.* **351–352** 247–63

[23] Morel F M M, Kraepiel A M L and Amyot M 1998 The chemical cycle and bioaccumulation of mercury *Annu. Rev. Ecol. Evol. Syst.* **29** 543–66

[24] Kozak N, Ahonen S A, Keva O, Østbye K, Taipale S J, Hayden B and Kahilainen K K 2021 Environmental and biological factors are joint drivers of mercury biomagnification in subarctic lake food webs along a climate and productivity gradient *Sci. Total Environ.* **779** 146261

[25] Arctic Monitoring and Assessment Programme 2021 2021 AMAP mercury assessment *Summary for Policy-Makers* (Arctic Monitoring and Assessment Programme (AMAP)) pp 1–16 (available at: www.amap.no/documents/download/6758/inline)

[26] Basu N, Abass K, Dietz R, Krümmel E, Rautio A and Weihe P 2022 The impact of mercury contamination on human health in the Arctic: a state of the science review *Sci. Total Environ.* **831** 154793

[27] Osterwalder S, Bishop K, Alewell C, Fritsche J, Laudon H, Åkerblom S and Nilsson M B 2017 Mercury evasion from a boreal peatland shortens the timeline for recovery from legacy pollution *Sci. Rep.* **7** 16022

[28] St Pierre K A, Zolkos S, Shakil S, Tank S E, St Louis V L and Kokelj S V 2018 Unprecedented increases in total and methyl mercury concentrations downstream of retrogressive thaw slumps in the Western Canadian Arctic *Environ. Sci. Technol.* **52** 14099–109

[29] Zolkos S *et al* 2020 Mercury export from Arctic great rivers *Environ. Sci. Technol.* **54** 4140–8

[30] Brabets T P, Wang B and Meade R H 2000 Environmental and Hydrological Overview of the Yukon River Basin, Alaska and Canada 99-4204 (U.S. Geological Survey) (https://doi.org/10.3133/wri994204)

[31] UAF, USACE Alaska District and USACE CRREL 2019 *Statewide Threat Assessment: Identification of Threats from Erosion, Flooding, and Thawing Permafrost in Remote Alaska* INE 19.03 (Denali Commission) (available at: www.denali.gov/wp-content/uploads/2019/11/Statewide-Threat-Assessment-Final-Report-20-November-2019.pdf)

[32] U.S. Army Corps of Engineers 2009 *Alaska Baseline Erosion Assessment: Study Findings and Technical Report* (U.S. Army Corps of Engineers Alaska District)

[33] Rowland J C, Schwenk J P, Shelef E, Muss J, Ahrens D, Stauffer S, Pilliouras A, Crosby B, Chadwick A, Douglas M M and Kemeny P C 2023 Scale-dependent influence of permafrost on riverbank erosion rates *J. Geophys. Res. Earth Surf.* **128** e2023JF007101

[34] Yukon River-Inter-Tribal Watershed Council 2022 *YRITWC's IGAP Map*

[35] Douglas M *et al* 2023 Geomorphic Mapping and Permafrost Occurrence on the Koyukuk River Floodplain near Huslia *Office of Scientific and Technical Information* (https://doi.org/10.15485/2204419)

[36] Pastick N J *et al* 2015 Probabilistic estimates of the distribution of near-surface permafrost in Alaska 2015 U.S. Geological Survey Science Data Catalog (https://doi.org/10.5066/F7C53HX6)

[37] Earthstar Geographics LLC SIO and TomTom n.d. (Microsoft Bing Maps)

[38] Maxar Technologies, CNES / Airbus and Landsat / Copernicus n.d. (Google Earth)

[39] USGS-Mercury Research Laboratory 2006 Analysis of Total Mercury in Solid Samples by Atomic Adsorption following Direct Combustion with the Nippon MA-2 Mercury Analyzer (U.S. Geological Survey) pp 1–10 (available at: https://d9-wret.s3.us-west-2.amazonaws.com/assets/palladium/production/s3fs-public/atoms/files/HgT%20in%20solids%20by%20Nippon%2C%202016.pdf)
[40] Smith M I *et al* 2024 Mercury content in floodplain sediments from the Yukon River Basin, Alaska, 2022 *Arctic Data Center* (https://doi.org/10.18739/A2FX74076)
[41] Ke Y *et al* 2024 Organic carbon content in floodplain sediments from the Yukon River Basin, Alaska Arctic Data Center (https://doi.org/10.18739/A22R3NZ79)
[42] Miall A D 2006 *The Geology of Fluvial Deposits* (Springer) (https://doi.org/10.1007/978-3-662-03237-4)
[43] Douglas M M, Li G K, Fischer W W, Rowland J C, Kemeny P C, West A J, Schwenk J, Piliouras A P, Chadwick A J and Lamb M P 2022 Organic carbon burial by river meandering partially offsets bank erosion carbon fluxes in a discontinuous permafrost floodplain *Earth Surf. Dyn.* **10** 421–35
[44] Geyman E *et al* 2024 Quantifying river migration rates in the Yukon River Watershed from optical satellite imagery, Alaska, 2016-2022 *Arctic Data Center* (https://doi.org/10.18739/A2WW7719J)
[45] Dietrich W E, Smith J D and Dunne T 1979 Flow and sediment transport in a sand bedded meander *J. Geol.* **87** 305–15
[46] Mason J and Mohrig D 2019 Differential bank migration and the maintenance of channel width in meandering river bends *Geology* **47** 1136–40
[47] Repasch M, Scheingross J S, Hovius N, Lupker M, Wittmann H, Haghipour N, Gröcke D R, Orfeo O, Eglinton T I and Sachse D 2021 Fluvial organic carbon cycling regulated by sediment transit time and mineral protection *Nat. Geosci.* **14** 842–8
[48] Repasch M, Wittmann H, Scheingross J S, Sachse D, Szupiany R, Orfeo O, Fuchs M and Hovius N 2020 Sediment transit time and floodplain storage dynamics in alluvial rivers revealed by meteoric ^{10}Be *J. Geophys. Res. Earth Surf.* **125** e2019JF005419